Astronomical and Astrophysical Transactions (*AApTr*), 2026, Vol. 36, Issue 1, pp. 73–90,
ISSN 1055-6796, Photocopying permitted by license only, ©Cambridge Scientific Publishers

Star-forming ring fueling AGN in the galaxy NGC 5347

I.S. Proshina[1,*], D.V. Oparin[2]

[1]*Sternberg Astronomical Institute of the Lomonosov Moscow State University, University av. 13, Moscow, 119234 Russia*
[2]*Special Astrophysical Observatory of the Russian Academy of Sciences, Nizhnij Arkhyz, 369167 Russia*

Received 1 December, 2025; accepted 10 December, 2025

We obtained for the ring galaxy with a strong bar and AGN NGC 5347 the narrowband images in the Hα, [NII]λ6583, and [OIII]λ5007 emission lines. We diagnosed two brightest clumps at the center and near to it excited by the AGN, two fainter clumps at the ends of the circumnuclear dust spirals, which could potentially feed the AGN, and sixty star-forming regions in a ring-like area between 21 and 44 arcsec from the center. We found that an oxygen abundance of the ionized gas in the star-forming regions varies in the range from 8.42±0.03 to 8.59±0.06 dex, demonstrating a correlation with the surface density of the modern rates of star formation in these clumps and an anticorrelation with distance from the center. The surface density of modern star formation rates also decreases with increasing distance from the center. Modern star formation in the ring is already fading.

Keywords: Galaxies: evolution – galaxies: star formation – galaxies: Seyfert – galaxies: jets – galaxies: individual: NGC 5347

1 Introduction

NGC 5347 (or UGC 8805) is a long-studied Seyfert type 2 galaxy with a bar, an inner ring from which spirals extend, and an outer open ring (see Figure 1). According to the NASA/IPAC Extragalactic Database (NED[1]), its morphological type is (R′)SB(rs)ab, its system velocity is 2368±2 km/s and its distance from us is 33.3 Mpc. The absolute magnitude in the B-band is $M_B = -19.75^m$, according to Lyon-Meudon Extragalactic Database (LEDA[2]). The nearest neighbor is the spiral galaxy PGC 49476 at a projected distance of about 404 kpc. According to the WHISP survey (Noordermeer et al., 2005), the galaxy is embedded in a huge disk of atomic hydrogen with a radius

*Email: ipro@sai.msu.ru
[1]`http://ned.ipac.caltech.edu/`
[2]`https://leda.univ-lyon1.fr/`

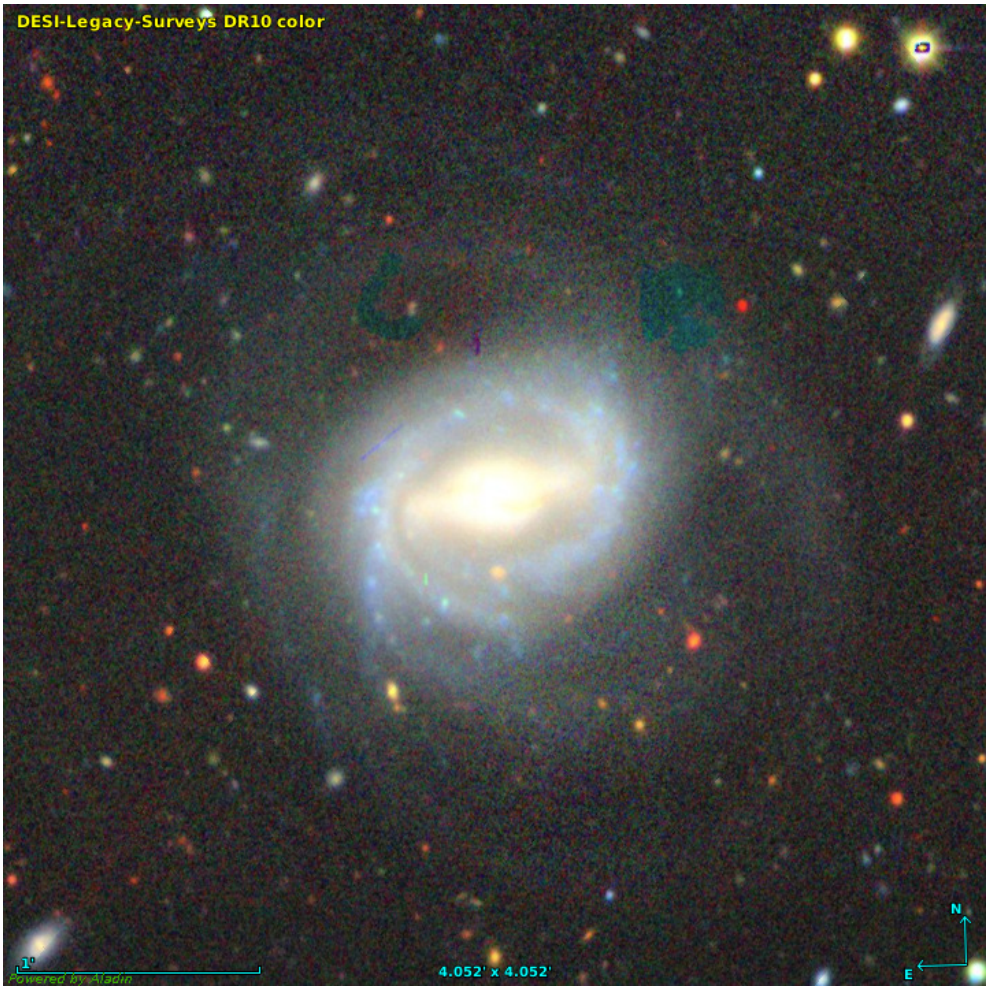


Figure 1 Optical composite-color image of the galaxy NGC 5347 from the Legacy Survey (Dey et al., 2019).

of $R_{HI} = 137$ arcsec (it is a radius where the face-on corrected surface density falls below a value of 1 $M_\odot$ pc^{-2}), which significantly exceeds the optical radius of the galaxy ($R_{25} = 51$ arcsec), and a mass of 4.34×10^9 $M_\odot$. However, the ALFALFA survey (Haynes et al., 2018) provides a lower mass estimate: lg $M_{HI}[M_\odot] = 9.58 \pm 0.07$. The amount of molecular gas is lg $M_{H_2}[M_\odot] = 8.82 \pm 0.15$ (Salvestrini et al., 2022; Maiolino et al., 1997). The logarithm of galaxy stellar mass inferred by Leroy et al. (2019) is lg $M_*[M_\odot] = 10.09 \pm 0.11$. At the center of the galaxy is a supermassive black hole, the logarithm of whose mass is lg $M_{BH}[M_\odot] = 6.73 \pm 0.55$ (Izumi et al., 2016). Comprehensive study of an X-ray emission based on archival data from *Suzaku*, *Chandra*, and *NuSTAR* performed by Kammoun et al. (2019) showed the existence of a Compton-thick source near the central engine of this AGN: soft X-rays are associated with thermal diffuse emission from extended regions, hard X-rays are de-

termined by reprocessed emission from Compton-thick material. However, Thean et al. (2000) according to the results of 0.25-arcsec-resolution radio observations at the VLA classified NGC 5347 as a single unresolved source (i.e. without linear structure).

One of the first thorough studies of NGC 5347, consisting of narrowband Hα+[NII] photometry and long-slit spectroscopy at $PA = 25°.5$, was performed by González Delgado & Pérez (1996). Then, Saburova et al. (2011) performed multiband (B, V, and R) photometry, including isophote analysis and surface brightness profile decomposition. The decomposition based on S^{4}G data is given in the ARRAKIS atlas (Comerón et al., 2014), according to which the position angles of the bar and major axis of the inner ring are $PA_{bar} = 100°.9$ and $PA_{inner\ ring} = 105°.7$, respectively. Long-slit spectroscopy in the wavelength range from 4800 Å to 5570 Å at three slit positions: $PA = 103°$, $PA = 120°$, and $PA = 30°$ was performed by Saburova et al. (2017).

2 Observations and archival data

We obtained the narrowband images of the NGC 5347 in the emission lines Hα, [NII]λ6583, [OIII]λ5007 and in the nearby red and green parts of the continuum on the 2.5-m telescope of the Caucasus Mountain Observatory of the Sternberg Astronomical Institute of Moscow State University (Shatsky et al., 2020) using a tunable photometer with a 13 Å bandwidth filter, MaNGaL (Moiseev et al., 2020), on 2023 April 18 and 24–25 with seeing 1.5–1.8 arcsec and 2–2.5 arcsec, respectively. The total exposure times are 1500 s, 3300 s, 3600 s, 1800 s and 2400 s, respectively. The scale of all images is 0.33 arcsec/px (1×1 binning). Primary data reduction and fluxes calibration were done in a routine manner according to Moiseev et al. (2020).

The derived intensity maps of the emission Hα, [NII]λ6583, and [OIII]λ5007 lines with continuum subtracted are shown in Figures 2a–c. The two brightest clumps in all narrowband images are located in the center and at a distance of 3.7 arcsec from it to the northeast. The fainter clumps are organized into a broad ring-like structure between 21 and 44 arcsec from the galaxy's center, with several more faint clumps visible outside the outer edge of the ring, and two small clumps visible outside the inner edge of the ring, closer to the center.

To provide additional information about the state of the gas in the two central clumps, we used a long-slit spectrum from the archive of the 6-m telescope BTA of the Special Astrophysical Observatory of the Russian Academy of Sciences, obtained on 2016 May 11 (PI: Saburova A.S.) at slit position $PA = 30°$, which intersects them, with seeing of 3 arcsec and a total exposure time of 1866 s. This spectrum was obtained using the SCORPIO universal focal reducer (Afanasiev & Moiseev, 2005) with the VPHG2300G grism which provided the spectral range of 4800–5570 Å , spectral resolution $R \approx 2200$ and reciprocal dispersion of 0.38 Å/pixel. The scale along the slit is 0.357 arcsec/pixel. We performed standard primary data reduction, which included the bias subtraction, line curvature and flat-field corrections, linearization, and night sky subtraction, and then we used Gaussian fitting for analysis.

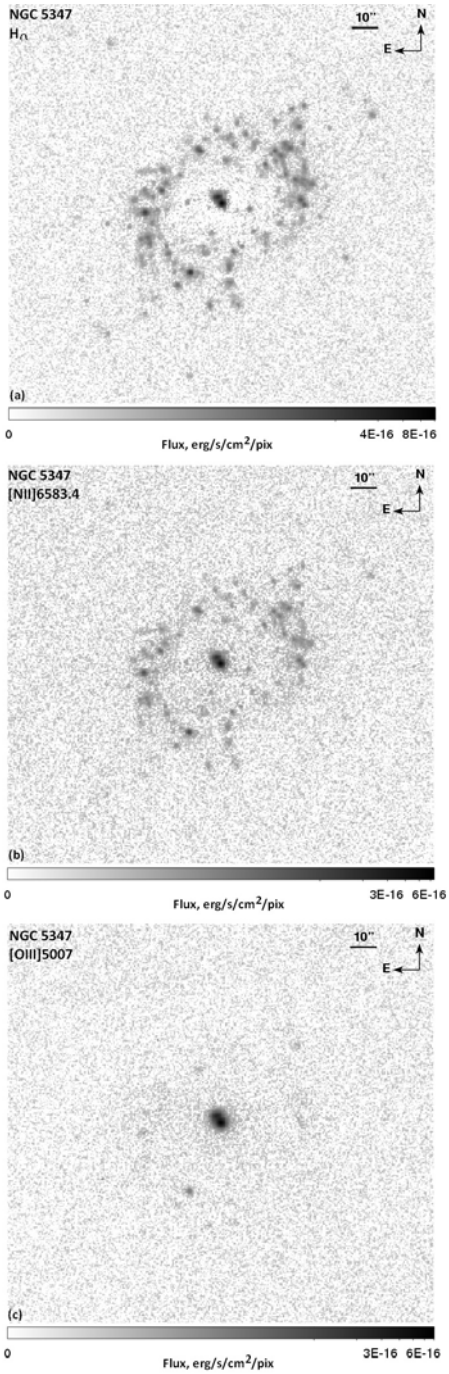


Figure 2 Intensity maps for NGC 5347 obtained with the MaNGaL in narrow emission lines: (a) Hα, (b) [NII]λ6583, (c) [OIII]λ5007 with continuum subtracted. A logarithmic brightness scale is applied.

3 Data analysis and results

3.1 Differences in ionized gas excitation mechanisms

To determine the mechanisms of excitation of ionized gas, we constructed several diagnostic maps. The map of equivalent widths of the Hα emission line (Figure 3) was constructed by correcting the intensity map of the Hα emission line for the partial contribution of emission from neighboring lines of the nitrogen doublet [NII]$\lambda\lambda$6548,6583, as described by Moiseev et al. (2020), multiplying by the filter bandwidth (13 Å) and dividing by the image in the neighboring continuum. Lacerda et al. (2018) proposed an empirical criterion of EW(Hα) $\geq$ 14 Å to identify regions where star formation dominates. Figure 3 shows that approximately fifty regions of different shapes satisfying this criterion are located predominantly in a ring-like area at distances from 21 to 44 arcsec from the center. In addition, this criterion is satisfied by two bright clumps at the center and at a distance of 3.7 arcseconds to the northeast, two less bright

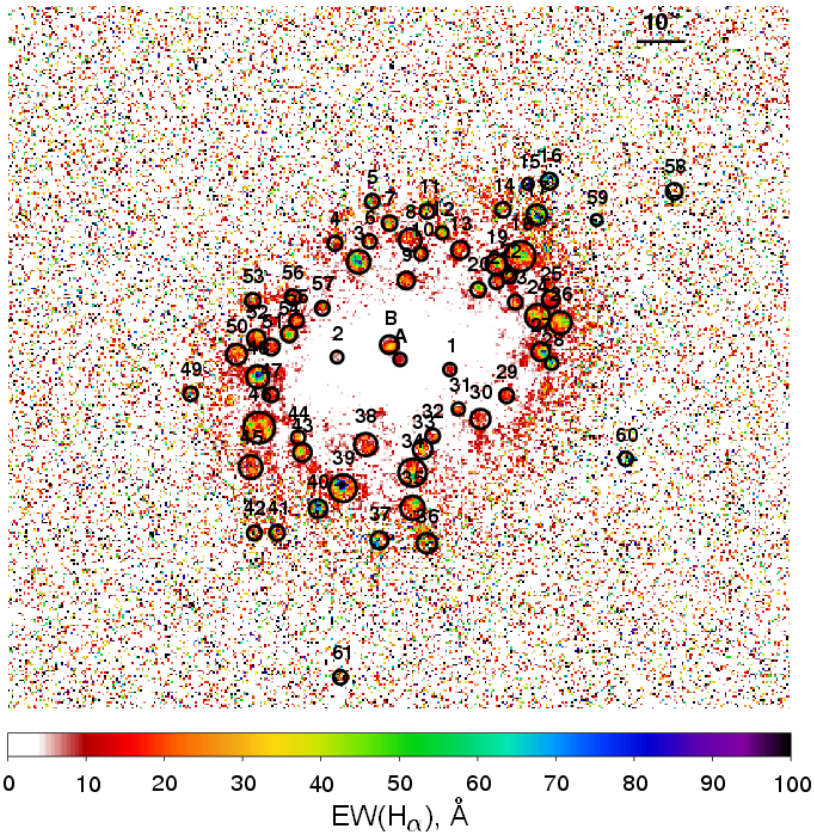


Figure 3 EW(Hα) diagnostic map for NGC 5347 with diagnosed star-forming regions marked by *numbered black apertures* and AGN-excited regions denoted by *black apertures with capital letters.*

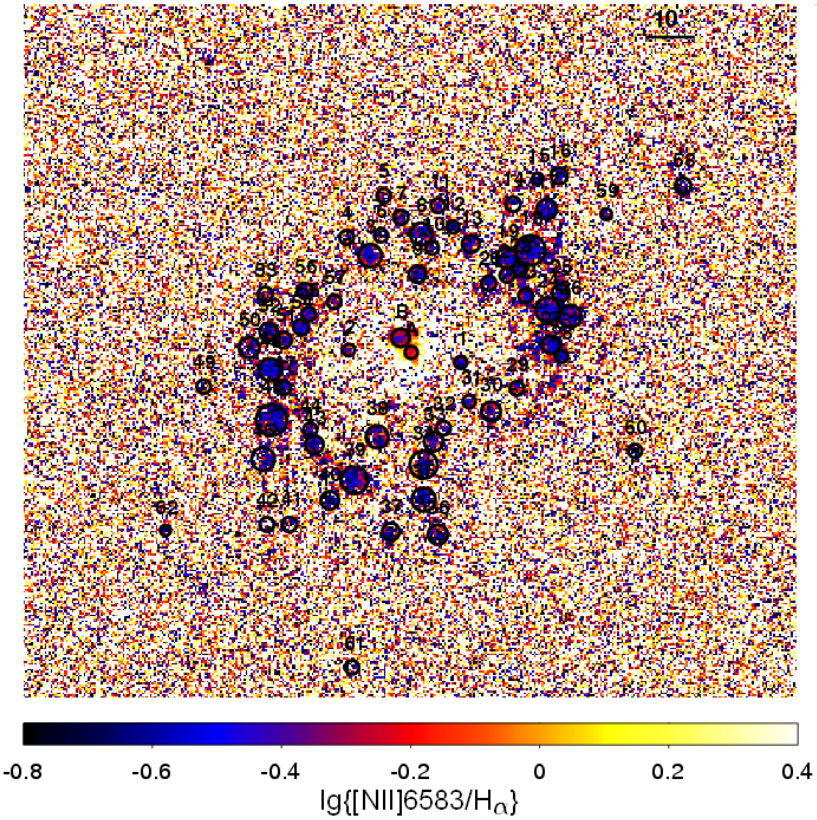


Figure 4 lg([NII]6583/Hα) diagnostic map for NGC 5347 with diagnosed star-forming regions marked by *numbered black apertures* and AGN-excited regions denoted by *black apertures with capital letters.*

clumps in the gap between the ring and the center, and several small faint clumps beyond the outer edge of the ring. We used circular apertures to select clumps in which the median value of the EW(Hα) satisfies this criterion. The sizes of the selected clumps, corrected for the seeing, varies in the range from 1.3 arcsec to 6 arcsec, corresponding to the physical sizes of 200–1000 pc (at the adopted distance to the galaxy of 33.3 Mpc).

The lg([NII]6583/Hα) map (Figure 4) was constructed by dividing the [NII]λ6583 and Hα emission line intensity maps by each other, per-pixel calibrating the ratio according to the calibration curve from Moiseev et al. (2020, see Fig. 5, right) and taking the logarithm of this ratio. We superimposed the apertures of the clumps identified in the EW(Hα) map on this map, and they matched the clumps visible on this map. As can be seen from Figure 4, all clumps except the two bright ones in the center satisfy the criterion lg([NII]6583/Hα) < -0.3, which corresponds to HII regions in the BPT diagram from Kewley et al. (2006). For the two clumps in the center, the value lg([NII]6583/Hα) > -0.3 corresponds to either mixed excitation or ionization from AGN. To clarify this, we need to construct the BPT diagram.

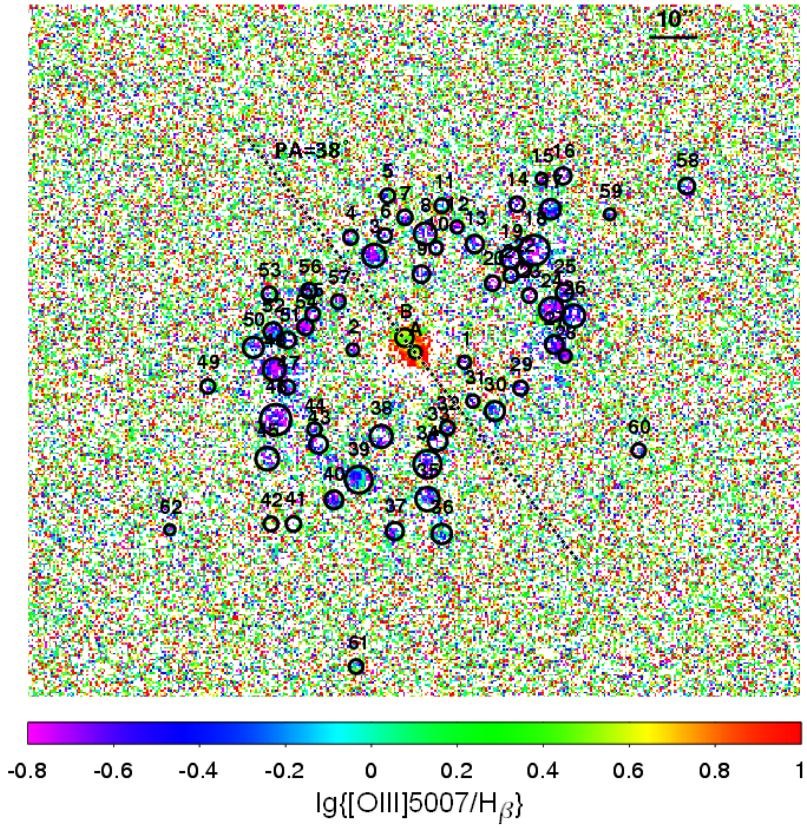


Figure 5 lg([OIII]5007/Hβ) diagnostic map constructed with assumed constant value of Hα/Hβ = 2.86 for NGC 5347 with diagnosed star-forming regions marked by *numbered black apertures* and AGN-excited regions denoted by *black apertures with capital letters*.

To plot the values on the BPT diagram, it is necessary to know the value of lg([OIII]5007/Hβ), but a narrowband image in the Hβ emission line was not obtained. Therefore, to construct a map in the Hβ emission line, we applied to Hα-map a constant Balmer decrement of 2.86, characteristic of star-forming regions diagnosed in the ring-like area, but under the assumption of its ubiquity (which is obviously incorrect). We then divided the [OIII]λ5007 and the Hβ emission line intensity maps by each other, took the logarithm of this ratio at each pixel, and derived the lg([OIII]5007/Hβ) map (Figure 5). As can be seen, this map also shows clumps in the ring-like area with values of lg([OIII]5007/Hβ) < -0.4 characteristic for the star formation process, but in the center two clumps and conical structure stand out with a lg([OIII]5007/Hβ) > 0.2 values indicating on AGN, even under the incorrect assumption of the Balmer decrement for this circumnuclear region.

However, in order to plot the correct values of the logarithms of the flux ratios in the emission lines on the BPT diagram (Figure 6), we adopted the Balmer decrement value of 4.94 for two clumps in the circumnuclear region, derived from the SDSS spectrum, which was obtained just in the central small aperture, and the logarithm values

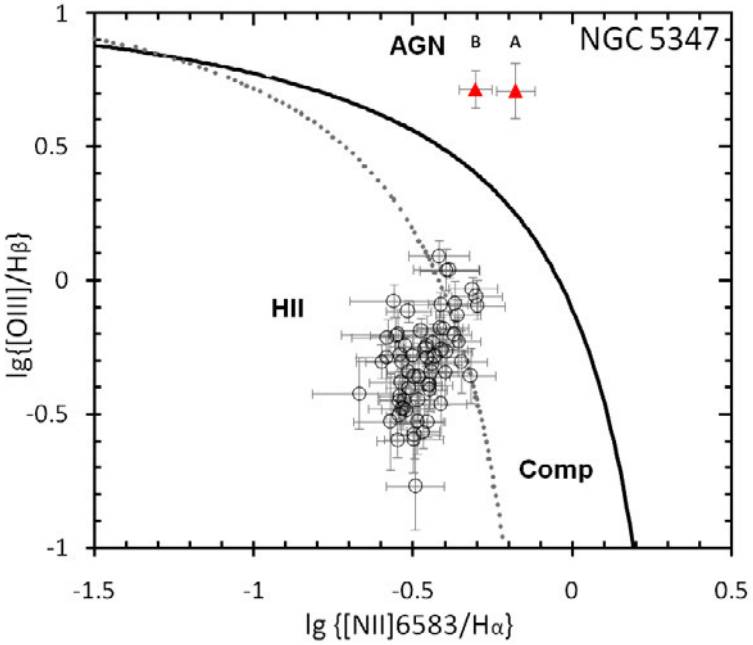


Figure 6 The BPT diagram for clumps in the galaxy NGC 5347. The theoretical model curve and the empirical boundary curve are constructed using the equations from Kewley et al. (2006) and are shown as solid and dotted lines, respectively. Clumps from ring-like area are marked by *open circles*. The state of the ionized gas in the two central clumps was estimated by using Balmer decrement value of 4.94 from SDSS spectra and marked by *red triangles*.

for the clumps from the ring-like area were taken from the lg([OIII]5007/Hβ) map by superimposing the apertures identified from the EW(Hα) and lg([NII]6583/Hα) maps.

As can be seen from Figure 6, only two gas clumps – one in the center (clump A) and one 3.7 arcsec to the northeast of it (clump B) – are excited by radiation from the active nucleus; in the remaining sixty-two clumps, the gas is ionized by current star formation. This means we can estimate the metallicity of the gas and rates of current star formation in these clumps, as will be shown in Subsections 3.3 and 3.4.

3.2 Two kinematically decoupled components of ionized gas at the center

We performed our own analysis of the long-slit spectrum in the spectral range of 4800–5570 Å along the $PA = 30°$ direction to study the gas state almost along the jet, taking this spectrum from the archive of the 6-m BTA telescope of the Special Astrophysical Observatory of the Russian Academy of Sciences (PI: Saburova A.S.). We identified the blue-wing asymmetry in the circumnuclear region and picked out two gas components with different kinematics (see Figures 7a–d): one – narrow (with FWHM of about 75–280 km/s, corrected for the instrumental value of FWHM), the other – broader (with FWHM of about 300–780 km/s, corrected for the instrumental

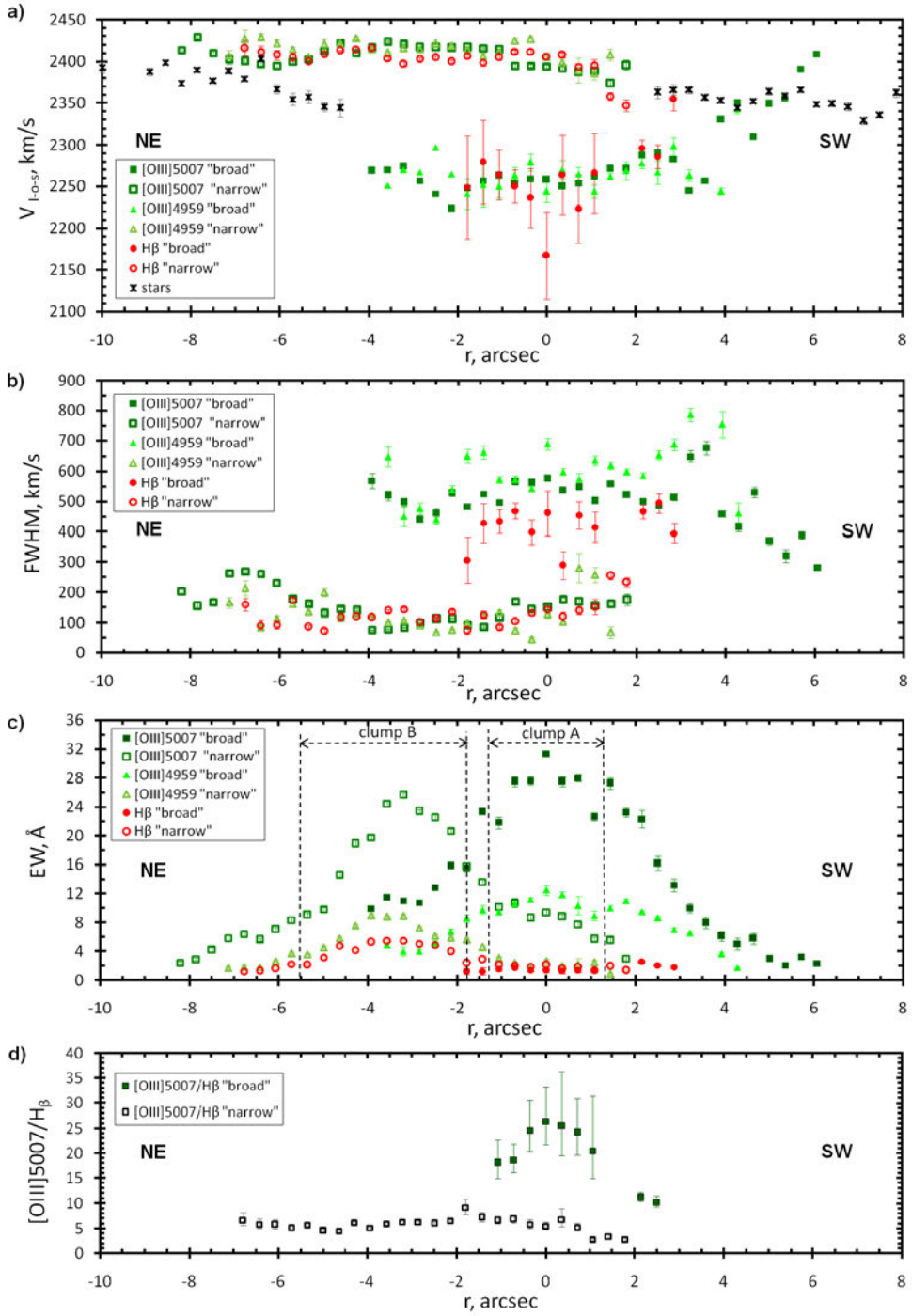


Figure 7 Variations in the line-of-sight velocities (a), FWHM (b), equivalent width (c), and [OIII]λ5007/Hβ emission line fluxes ratios (d) for the narrow and broader components along the long slit $PA = 30^\circ$ in the galaxy NGC 5347.

value of FWHM). The peaks of the equivalent-width (EW) change profiles of the narrow component's emission lines [OIII]λ5007, [OIII]λ4959, and Hβ along the slit coincide with the center of clump B. And the peaks of the EW change profiles of the broader component's emission lines [OIII]λ5007, [OIII]λ4959, and Hβ are located at the center of the galaxy, where we have marked clump A. These two components differ significantly in their line-of-sight velocities: the narrow component's median line-of-sight velocity is 2410 km/s along the entire extent where the narrow component is detected (from –8 arcsec in the northeast to +2 arcsec in the southwest), while the broader component of [OIII]λ4959, [OIII]λ5007 emission lines begins within the central region with a radius of 4 arcsec (and the broader component of Hβ emission line appears within the central region with a radius of 2 arcsec) with a median line-of-sight velocity of about 2270 km/s, i.e., it is gaseous outflow approaching us with line-of-sight velocity of 140 km/s. The presence of narrow and broad components in the center of the galaxy NGC 5347 was previously reported by González Delgado & Pérez (1996). Similar nuclear outflows have been observed in other galaxies with AGN (see Smirnova et al. (2006) and references therein). At a distance of 4 to 6 arcsec from the center to the southwest, the broader component gradually narrows and approaches the line-of-sight velocity of the narrow component. The [OIII]λ5007/Hβ emission line fluxes ratio for the narrow component is $\sim$ 6 with small variation throughout its extent (i.e. along the conical structure clearly visible in Figure 5); for the broader component, the reddening-corrected [OIII]λ5007/Hβ ratio is much higher, with a peak value of about 27 at the center.

We did not detect any emission lines along the slit in the direction $PA = 30^\circ$ outside the range indicated above (and plotted on the horizontal axes in Figures 7a–d). It is interesting to note, as can be seen from the diagnostic maps (Figures 3–5), that in the direction of the conical structure ($PA = 38^\circ$) there are no clumps on either side of the center in the ring-like area. We do not know the exact reason for this, but several explanations can be suggested: i) it is somehow related to the impact of the AGN jet, the cone of which is projected onto the disk in this direction, however, the ring is located several times further than the length of the observed conical structure; ii) it may be related to the influence of the bar, since in the resonant rings an increase in density is observed at the ends of the bar, and a rarefaction of density is observed in the midway, however, the $PA_{bar} = 101^\circ$ (Comerón et al., 2014), so the direction $PA = 38^\circ$ is not perpendicular to the bar; iii) the direction $PA = 38^\circ$ is close to the position of the major axis of the HI disk (unfortunately, Noordermeer et al. (2005) did not provide an exact value for the position angle of the HI disk; we estimated it from maps from the WHISP survey to be $PA = 48^\circ$); possibly along this direction the stellar disk and the disk of atomic hydrogen intersect.

We confidently detected the presence of the stellar component by cross-correlating with spectrum of K-gaint star (HD 20893) within a radius of about 15 arcsec from the center, excluding the central region within the range from –4.5 arcsec in the northeast to +2.5 arcsec in the southwest (see Figure 7a), since there are no cross-correlation peaks. This means that the northeastern cone of the relativistic jet is located above the plane of the stellar disk, but close to this plane, so one of the star-forming complexes (clump B), moving in the plane of the galactic disk, entered the cone of the jet; and its southwestern conical part is hidden from us by the dusty galactic disk, as well as the AGN in the very center is hidden from us by dust protruding above the

disk. Clump A corresponds to a Compton-thick source and the conical structure with clump B at the base corresponds to a Compton-thin source revealed by Kammoun et al. (2019) in the X-ray spectrum of the galaxy NGC 5347.

3.3 Comparison of current and recent star formation rates

For each star-forming clump, we calculated the rates of current and recent star formation using formulas from Kennicutt & Evans (2012) and based on the measured fluxes in the Hα emission line from the intensity map (Figure 2a) and the ultraviolet fluxes in the FUV and NUV bands from the GALEX space telescope images (Figure 8).

We used two pairs of UV images obtained by the GALEX space telescope under the "AIS 238 0001 sg19" and "AIS 238 0001 sg26" programs, which we took from the Mikulski Archive for Space Telescopes[3]. For the first program, the exposures of images in the FUV and NUV bands were 59 s and 272 s, respectively; for the second program, the exposures were 91 s and 288.05 s in the FUV and NUV bands, respectively. We applied a correction for the extinction in our Galaxy in the direction of NGC 5347, taking $A_B = 0.075^m$ (according to the NED database) and also a correction for dust absorption in the galaxy NGC 5347 itself, for which we used an image in the W4 band obtained by the WISE space infrared telescope and taken from the IRSA[4]. A detailed description of the SFR calculation is given in our previous work (Proshina et al., 2025).

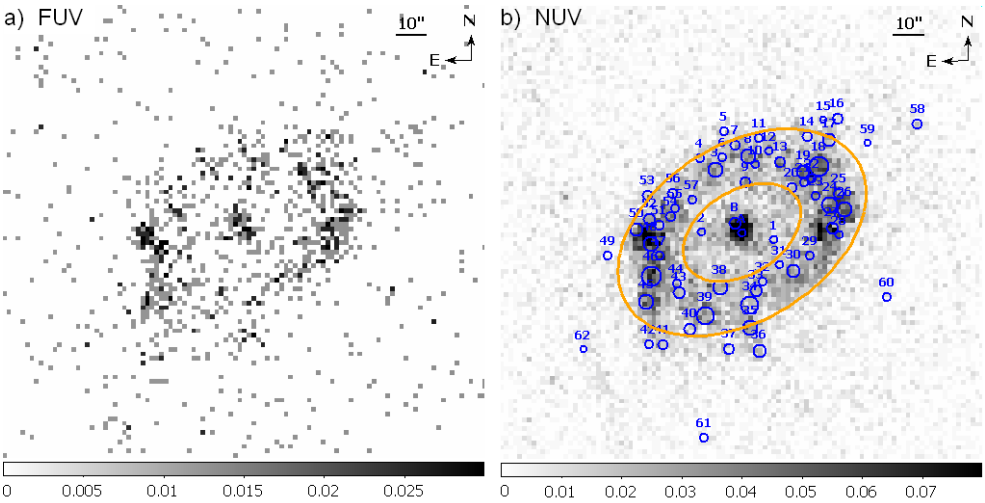


Figure 8 UV images for NGC 5347 in the FUV-band (a) and NUV-band (b) with sites of clumps superimposed (*blue apertures*). The integral fluxes were measured in an annular aperture marked in *orange*.

For comparison, we plotted on the vertical axis the surface densities of the star formation rates calculated from the fluxes in the Hα emission line and in the FUV and

[3] https://galex.stsci.edu/GR6/
[4] https://irsa.ipac.caltech.edu/applications/wise/

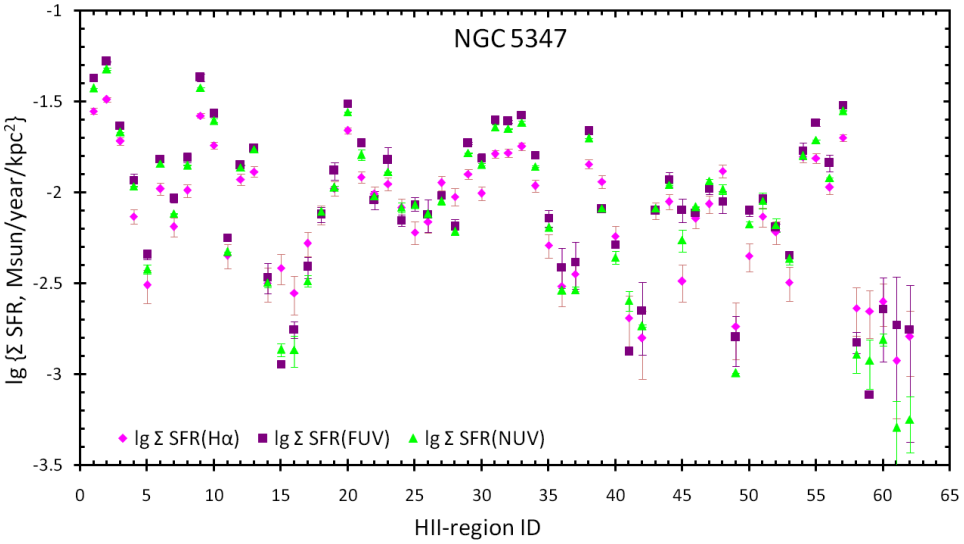


Figure 9 Comparison of the values of the surface densities of star formation rates for each star-forming clump, estimated by three indicators: the Hα flux (*magenta*), FUV flux (*purple*), NUV flux (*green*).

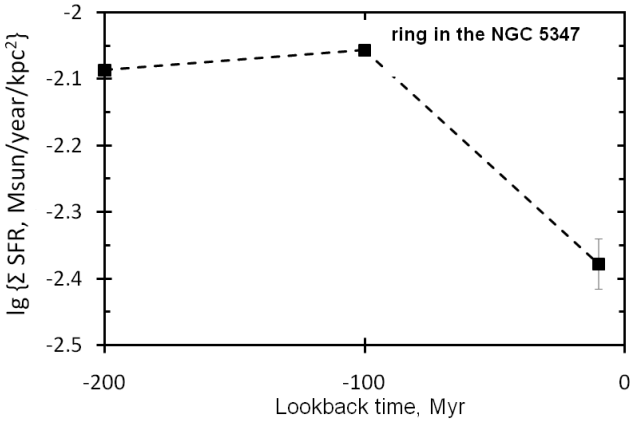


Figure 10 History of modern star formation in the ring of the galaxy NGC 5347.

NUV bands for each clump (Figure 9). As can be seen, in the overwhelming majority of clumps, star formation is already fading, since the Σ_{SFR}s values calculated from the Hα fluxes are lower than values calculated from UV fluxes.

As can be seen from Figure 10, the same conclusion is reached by comparing the integral rates of star formation estimated from the integral fluxes from the entire star-forming ring (outlined by the *orange* annular aperture in Figure 8) on three time scales: up to 10 million years ago (Hα fluxes), up to 100 million years ago (fluxes in the FUV band), up to 200 million years ago (fluxes in the NUV band).

The integral rate of star formation over the past 200 million years, calculated from the integral flux in the NUV band, is 1.000±0.003 $M_\odot$/yr. The current rate of star formation, calculated from the integral Hα emission line flux in the ring aperture, is 0.66±0.06 $M_\odot$/yr.

3.4 Some anticorrelations and correlations

We calculated the oxygen abundance (gas metallicity) 12+lg(O/H) using the *O3N2* indicator in the calibration by Marino et al. (2013) for each clump in which we diagnosed current star formation. It ranges from 8.42 ± 0.03 dex in the clump 61 to 8.59 ± 0.05 dex in the clump 22 (where uncertainties based on the errors in measuring the fluxes in the emission lines) with a mean of 8.50 ± 0.03 dex. This is ~ 0.2 dex less than the solar value and is typical for star-forming regions in the rings of lenticular galaxies (Proshina et al., 2019).

We found a correlation between the gas metallicity and the surface density of star formation rates calculated from both Hα and UV fluxes (Figure 11).

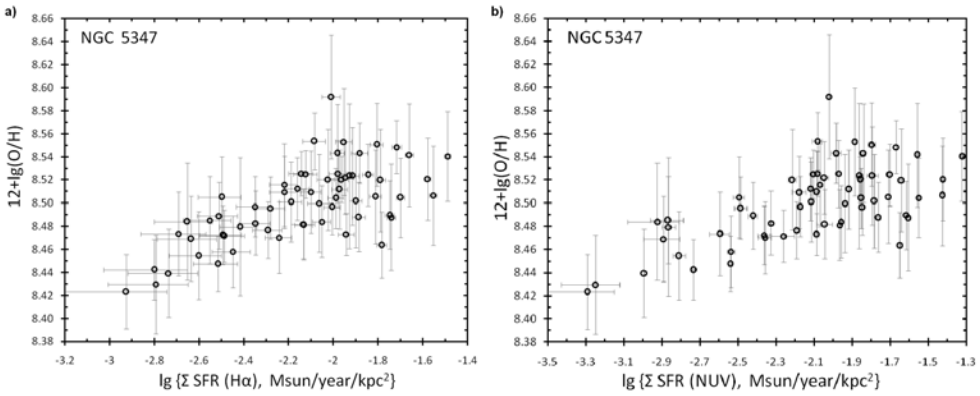


Figure 11 Correlation of gas metallicity and surface density of star formation rates calculated from Hα (a) and NUV (b) fluxes in each of 62 HII regions.

However, a decrease in the gas metallicity and the surface density of star formation rates is observed with increasing distance from the center of the galaxy NGC 5347 (Figure 12). We used the value of semimajor axis as a measure of the distance from the center to each clump.

As can be seen, smaller, less metallicity clumps are observed at the periphery of the ring, and a few are found outside it in the spirals. Within the ring, some clumps merge into conglomerates (Figures 3–5). As the distance to the galactic center decreases, metallicity and star formation rates increase. This indicates that gas processed and ejected by stars remains within the ring or even inside individual star-forming clumps, concentrating toward inner boundary of the ring, perhaps, by moving the clumps themselves. Apparently, some clumps exit the ring, moving further toward the galactic center (see Figure 13 and Section 4).

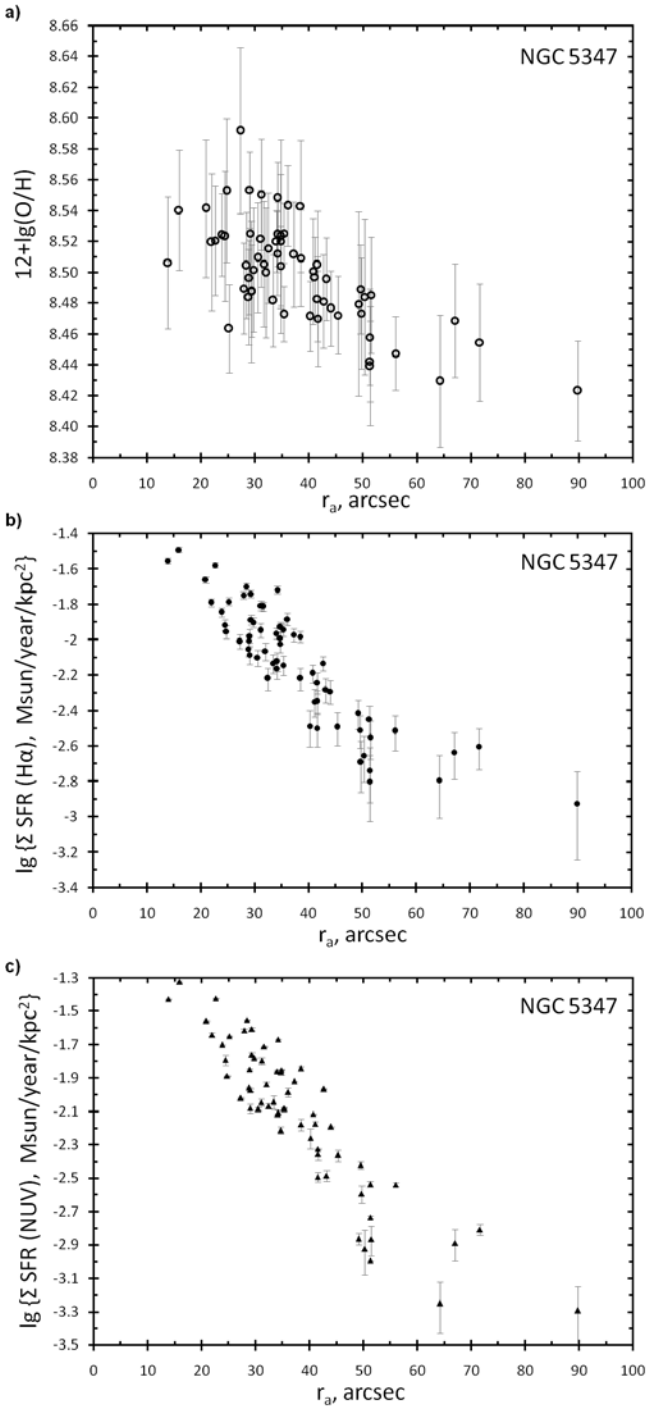


Figure 12 Decrease in the gas metallicity (a) and the surface density of star formation rates calculated from Hα fluxes (b) and NUV fluxes (c) with increasing distance from the center of the galaxy NGC 5347.

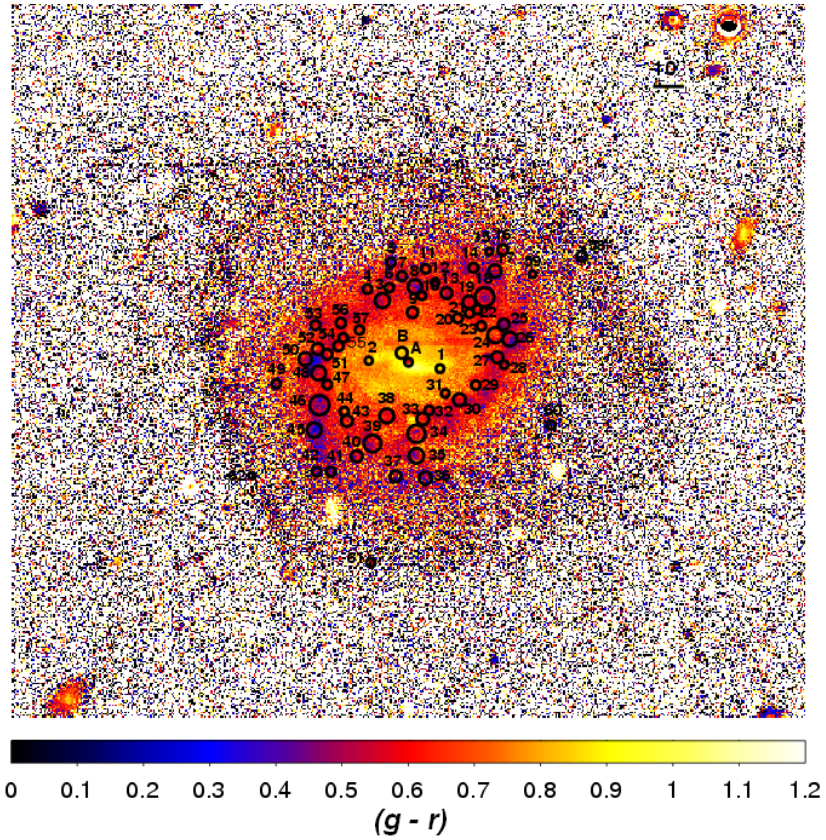


Figure 13 Color index (g-r) map for NGC 5347 with sites of clumps superimposed.

4 Discussion of the fueling mechanism for AGN in the galaxy NGC 5347

We constructed a color index (g-r) map of the galaxy NGC 5347 (Figure 13) using images from the Legacy Survey (Dey et al., 2019) and superimposed all clumps on it.

In Figure 13, two spiral arms of dust are clearly visible in circumnuclear area with star-forming clumps 1 and 2 at their ends. These dust spirals were previously clearly visible on the images obtained by Hubble Space Telescope (Martini et al., 2003a) and have been mentioned by Regan & Mulchaey (1999), Martini & Pogge (1999) as a possible feeding mechanism of AGN, but not universal (Martini et al., 2003b).

We have recognized the clumps which are very likely transported by spirals and will be fueling the AGN. However, the gas must lose angular momentum to move from the ring-like area several kiloparsecs away to the galactic center. This mechanism is likely dynamic friction between gravitationally bound gaseous star-forming clumps, which forces some of them out of the ring-like area toward the nuclear. For example, Smirnova et al. (2006) showed that in the case of the galaxy NGC 6104 a gaseous clouds can reach the AGN, providing fueling for it. Thus, our analysis of narrowband images *hint* that the gas is moving toward the center of NGC 5347 not as a gas flow,

but is spiraling in the form of clumps (or giant molecular clouds) ejected from the ring where they formed; thereby episodically feeding the supermassive black hole, which reveals itself in its episodic activity, i.e. such gaseous star-forming clumps are direct triggers of AGN activity. This detection refines the idea of a connection between mass accretion onto a supermassive black hole and star formation in circumnuclear disks proposed by Izumi et al. (2016).

5 Conclusions

For the galaxy NGC 5347, we obtained narrowband images in the emission lines Hα, [NII]λ6583, [OIII]λ5007 and in the nearby continuum, analyzed them, reanalyzed the archival optical spectrum (only the green part) and now summarize our findings.

- In the center of NGC 5347 and at a distance of 3.7 arcsec from it in the northeast, two most bright clumps are visible, the gas in which is ionized by the active galactic nucleus. In the central region with a radius of 2 arcsec, we confidently distinguished the broader component, which was identified as outflow with line-of-sight velocity of 140 km/s toward us. On the constructed diagnostic maps, in the direction $PA = 38°$ from the center to the northeast (coinciding with the direction of the relativistic jet from the AGN and projecting close to the position of the minor axis of the inner ring of the galaxy and close to the position of the major axis of the HI disk), a conical structure appears. In the same direction, the absence of clumps of star formation in the ring is noticeable.
- Gas ionized by O-B stars is concentrated primarily in a ring-like area at distances of 21 to 44 arcsec from the galactic center. There are several faint clumps of current star formation outside the outer edge of the ring, and two inside the ring project onto the ends of dust spirals that appear in the circumnuclear area on the color index map (g-r) of the galaxy NGC 5347 and could potentially serve as fuel for AGN.
- Star formation occurs in individual clumps of various shapes, 200–1000 pc in size, comparable to those observed in spiral and lenticular galaxies, at a rate of about 1 $M_\odot$/yr, that is typical for these types of galaxies, and is already fading.
- The metallicity of the gas in the HII regions varies in the range of 8.42–8.59 dex, which is typical for star-forming regions in the rings of lenticular galaxies, demonstrating a correlation with the surface density of rates of modern star formation in these clumps and an anticorrelation with distance from the center.

Thus, despite the extensive HI gas disk, intense star formation in the galaxy NGC 5347 is observed not in the spirals, but in a restricted area of the resonant inner ring (as Buta & Combes (1996) showed, the inner ring is formed at the ultraharmonic (1:4) resonance near the end of the bar), which means that only in this area are conditions created that provoke star formation.

ACKNOWLEDGEMENTS

The study was conducted under the state assignment of Lomonosov Moscow State University.

The authors thank A.V. Moiseev for the primary processing of observational data.

This work is based on the data obtained at the 2.5-meter telescope of the Caucasus Mountain Observatory of the Sternberg Astronomical Institute of the Moscow State University, data from the archive of the 6-m Big Telescope Alt-azimuthal of the Special Astrophysical Observatory of Russian Academy of Science, which is supported by the Ministry of Science and Higher Education of the Russian Federation, and on the public data of the SDSS (http://www.sdss3.org), Legacy Surveys (http://legacysurvey.org/) and GALEX (http://galex.stsci.edu/GR6/) surveys. Funding for SDSS-III has been provided by the Alfred P. Sloan Foundation, the Participating Institutions, the National Science Foundation, and the U.S. Department of Energy Office of Science. The Legacy Surveys imaging of the DESI footprint is supported by the Director, Office of Science, Office of High Energy Physics of the U.S. Department of Energy under Contract No. DE-AC02-05CH1123; by the National Energy Research Scientific Computing Center, a DOE Office of Science User Facility under the same contract; and by the U.S. National Science Foundation, Division of Astronomical Sciences under Contract No. AST-0950945 to NOAO. The NASA GALEX mission data were retrieved from the Mikulski Archive for Space Telescopes (MAST) at the Space Telescope Science Institute, which is operated by the Association of Universities for Research in Astronomy, Inc., under NASA contract NAS 5–26555. The WISE image used by us was taken from the NASA/IPAC Infrared Science Archive, which is operated by the California Institute of Technology, under contract with the National Aeronautics and Space Administration. We also used the NASA/IPAC Extragalactic Database (NED) which is operated by the California Institute of Technology, under contract with the National Aeronautics and Space Administration. We acknowledge the usage of the Lyon Extragalactic Database (HyperLEDA, http://leda.univ-lyon1.fr).

References

Afanasiev V. L. and Moiseev A.V. (2005) AstL, 31, 194
Buta R. and Combes F. (1996), Fundam. Cosm. Phys. 17, 95
Comerón S., Salo H., Laurikainen E., et al. (2014) A&A, 562, A121
Dey A., Schlegel D. J., Lang, D., et al. (2019) AJ, 157, 168
Haynes M. P. et al. (2018) ApJ, 861, 49
González Delgado R. M. and Pérez E. (1996) MNRAS, 280, 53
Izumi T., Kawakatu N., Kohno K. (2016) ApJ, 827, 81
Kammoun E. S., Miller J. M., Zoghbi A., et al. (2019) ApJ, 877, 102
Kennicutt R. C. and Evans N. J. (2012) ARA&A, 50, 531
Kewley L. J., Groves B., Kauffmann G., Heckman T. (2006) MNRAS, 372, 961
Lacerda E. A. D., Cid Fernandes R., Couto G. S., et al. (2018) MNRAS, 474, 3727
Leroy A. K., Sandstrom K. M., Lang D., et al. (2019) ApJS, 244, 24
Maiolino R., Ruiz M., Rieke G. H.; Papadopoulos, P. (1997) ApJ, 485, 552

Marino R. A., Rosales-Ortega F. F., Sánchez S. F., et al. (2013) A&A, 559, A114
Martini P. and Pogge R. W. (1999) AJ, 118, 2646
Martini P., Regan M. W., Mulchaey J. S., Pogge R. W. (2003a) ApJS, 146, 353
Martini P., Regan M. W., Mulchaey J. S., Pogge R. W. (2003b) ApJ, 589, 774
Moiseev A., Perepelitsyn A., Oparin D. (2020) Experimental Astronomy, 50, 199
Noordermeer E., van der Hulst J. M., Sancisi R., et al. (2005) A&A, 442, 137
Proshina I. S. and Oparin D. V. (2025) ApJ, 980, 118
Proshina I. S., Kniazev A. Yu., Sil'chenko O. K. (2019) AJ, 158, 5
Regan M. W. and Mulchaey J. S. (1999) AJ, 117, 2676
Saburova A. S., Bizyaev D. V., Zasov A. V. (2011) AstL, 37, 751
Saburova A. S., Katkov I. Y., Khoperskov S. A., et al. (2017) MNRAS, 470, 20
Salvestrini F., Gruppioni C., Hatziminaoglou E., et al. (2022) A&A, 663, A28
Shatsky N., Belinski A., Dodin A., et al. (2020) in Ground-Based Astronomy in Russia. 21st Century, ed. Romanyuk I. I. et al. (Nizhnij Arkhyz: SAO RAS), p.127, arXiv2010.10850
Smirnova A.A., Moiseev A.V., Afanasiev V. L. (2006) AstL, 32, 520
Thean A., Pedlar A., Kukula M. J., et al. (2000) MNRAS, 314, 573